Advanced Hybrid Supercapacitor Based on a Mesoporous Niobium Pentoxide/Carbon as High-Performance Anode

Eunho Lim,[†,▽] Haegyeom Kim,[§,▽] Changshin Jo,[‡,▽] Jinyoung Chun,[‡] Kyojin Ku,[§] Seongseop Kim,[‡] Hyung Ik Lee,[⊥] In-Sik Nam,[†,‡] Songhun Yoon,[∥,*] Kisuk Kang,[§,#,*] and Jinwoo Lee[†,‡,*]

[†]School of Environmental Science and Engineering, Pohang University of Science and Technology (POSTECH), Pohang, Kyungbuk 790-784, Republic of Korea, [‡]Department of Chemical Engineering, Pohang University of Science and Technology (POSTECH), Pohang, Kyungbuk 790-784, Republic of Korea, [§]Department of Materials Science and Engineering, Research Institute of Advanced Materials (RIAM), Seoul National University, 599 Gwanak-ro, Gwanak-gu, Seoul 151-742, Republic of Korea, [⊥]4-3, Agency for Defense Development, Yuseong, P.O. Box 35-4, 305-600 Daejeon, Republic of Korea, [∥]Department of Integrative Engineering, Chung-Ang University, 221, Heukseok-Dong, Dongjak-Gu, Seoul 156-756, Republic of Korea, and [#]Center for Nanoparticle Research, Institute for Basic Science (IBS), Seoul National University, Seoul 151-742, Republic of Korea. [▽]E. Lim, H. Kim, and C. Jo contributed equally to this work.

ABSTRACT Recently, hybrid supercapacitors (HSCs), which combine the use of battery and supercapacitor, have been extensively studied in order to satisfy increasing demands for large energy density and high power capability in energy-storage devices. For this purpose, the requirement for anode materials that provide enhanced charge storage sites (high capacity) and accommodate fast charge transport (high rate capability) has increased. Herein, therefore, a preparation of nanocomposite as anode material is presented and an advanced HSC using it is thoroughly analyzed. The HSC comprises a mesoporous Nb_2O_5/carbon (m-Nb_2O_5—C) nanocomposite anode synthesized by a simple one-pot method using a block copolymer assisted self-assembly and commercial activated carbon (MSP-20) cathode under organic electrolyte. The m-Nb_2O_5—C anode provides high specific capacity with outstanding rate performance and cyclability, mainly stemming from its enhanced pseudocapacitive behavior through introduction of a carbon-coated mesostructure within a voltage range from 3.0 to 1.1 V (*vs* Li/Li^+). The HSC using the m-Nb_2O_5—C anode and MSP-20 cathode exhibits excellent energy and power densities (74 W h kg^{-1} and 18 510 W kg^{-1}), with advanced cycle life (capacity retention: ~90% at 1000 mA g^{-1} after 1000 cycles) within potential range from 1.0 to 3.5 V. In particular, we note that the highest power density (18 510 W kg^{-1}) of HSC is achieved at 15 W h kg^{-1}, which is the highest level among similar HSC systems previously reported. With further study, the HSCs developed in this work could be a next-generation energy-storage device, bridging the performance gap between conventional batteries and supercapacitors.

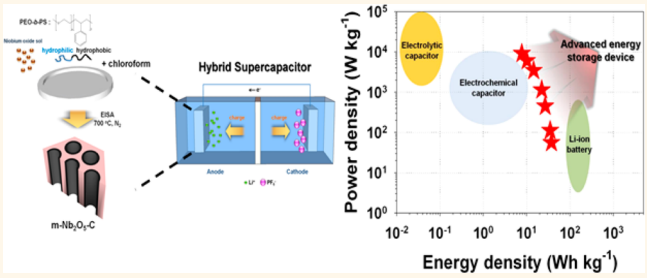

KEYWORDS: hybrid supercapacitors · Nb_2O_5 · pseudocapacitive properties · mesoporous materials · block copolymer-assisted self-assembly

The range of energy-storage device applications has expanded from portable electronics to large-scale energy-storage systems, including renewable energy storage and electricity transportation.[1−4] To fulfill the energy and power density requirements of energy applications, much research has been devoted to improving the performances of energy-storage devices such as lithium-ion batteries (LIBs) and supercapacitors (SCs).[5−8] However, despite their high energy densities (~150 W h kg^{-1}), LIBs have fundamental limitations such as low power densities and poor cycling lifetimes because they operate using faradaic reactions that involve ionic diffusion in a crystal framework.[9,10] In contrast, it is well-known that SCs provide high power (2−5 kW kg^{-1}) and have long cycling stabilities because they are based on fast physical adsorption/desorption of solvated ions at the electrode−electrolyte interface; however, they usually suffer from limited energy densities (3−6 W h kg^{-1}).[11,12] Recently, novel energy-storage

* Address correspondence to yoonshun@cau.ac.kr, matlgen1@snu.ac.kr, jinwoo03@postech.ac.kr.

Received for review April 9, 2014 and accepted August 18, 2014.

Published online August 19, 2014
10.1021/nn501972w

systems having the advantages of both LIBs and SCs have been proposed, namely, hybrid supercapacitors (HSCs).[11,13]

The concept of HSC is the combination of both energy-storage systems by using electrode materials of LIBs as anodes and carbonaceous electrodes of SCs as cathodes under organic electrolyte containing lithium salts.[14−17] Previous studies have shown that the energy and power densities of HSCs are comparable to, or even higher than, those of LIBs and SCs. However, the imbalance between the kinetics of the two electrodes is a problem that needs to be solved for commercial applications because, in general, anode kinetics using the faradaic lithium intercalation reaction is far more sluggish than that of cathodes using physical adsorption/desorption of electrolyte ions.[18,19] Therefore, it is vital to develop novel high-power anode materials to narrow the kinetics gap between two electrodes. In previous studies, nanostructured titanium-based anode materials such as TiO_2 and $Li_4Ti_5O_{12}$ have been extensively used in HSC systems because of their fast Li^+ insertion kinetics.[19,20] However, the relatively high redox potential (>1.5 V) over titanate electrodes is a major drawback, and leads to unnecessary loss of energy density.[21,22]

Niobium pentoxide (Nb_2O_5) is one of the most promising candidates for replacing conventional titanate electrodes. Recently, it has been demonstrated that Nb_2O_5 can deliver high power through a mainly pseudocapacitive reaction of Li^+ on the (near) surface of the electrode, accompanied by an intercalation reaction.[23,24] The Nb_2O_5 with pseudocapacitive reaction mechanism for charge storage could be very suitable as the anode of HSC systems because of its outstanding high power performance. This unique property of Nb_2O_5 could result in the harmonious electrochemical performance with electrical double-layer type cathode based on intrinsically fast physical adsorption/desorption of electrolyte ions. The high theoretical capacity (~200 mA h g^{-1}), which is higher than that of $Li_4Ti_5O_{12}$ (~175 mA h g^{-1}), is also advantageous in delivering high energy densities in HSC systems.[25−27] However, the application of Nb_2O_5-based anodes in HSCs has been hampered by both the low electrical conductivity and the difficulty to control optimum crystal structure.[24,28] The sluggish mobility of electrons in Nb_2O_5 should be further improved through surface modifications (*e.g.*, carbon coating). Although the nanocomposite of nanosized Nb_2O_5 nanocrystals and high conductive carbon nanotubes (CNTs) was prepared by Lu *et al.*, the specific capacity of pseudohexagonal Nb_2O_5/CNTs composite (calcined at 300 °C) was still not sufficient for the high-performance HSC system.[29] This low capacity was attributed to strong capacity-dependency on the crystal structure of Nb_2O_5 material. Among various crystal structures of Nb_2O_5, the orthorhombic phase has shown the highest specific capacity compared with other phases such as pseudohexagonal and amorphous phase.[24] However, nanoparticle aggregation is inevitable due to high calcination temperature (>600 °C) for the orthorhombic phase formation of Nb_2O_5. Particularly, HSC systems require the high-power anode materials in order to balance the kinetics gap between the slow faradaic anode and the fast electric double-layer type cathode. For the purpose of kinetics improvement of anode system, nanosized orthorhombic Nb_2O_5 material is highly advantageous. In spite of this merit, the synthesis of small-sized orthorhombic Nb_2O_5 has been recognized as one of the major challenges, mainly due to synthetic difficulties. For these reasons, the research on Nb_2O_5-based HSC systems has been rarely realized. Hence, one can expect that well-nanostructured orthorhombic Nb_2O_5 with carbon coating can produce high-performance anode for HSC system.

In addressing this issue, a key strategy is the one-pot synthesis of a mesoporous Nb_2O_5/carbon nanocomposite (denoted by m-Nb_2O_5−C). The m-Nb_2O_5−C is synthesized using a block copolymer [poly(ethylene oxide-*b*-poly(styrene)), PEO-*b*-PS] as a structure-directing agent.[30,31] The mesoporous material comprising nanocrystalline Nb_2O_5 could enhance the electrochemical activity originated from (i) particles of nanoscale regime, providing a shortened diffusion length and the large electrode−electrolyte interface area compared with the bulk structure; and (ii) enhanced ionic transportation through the mesopores.[32−34] In addition, (iii) the uniform carbon layers formed by thermal decomposition of the PS block during heat-treatment not only maintain the mesostructure comprising orthorhombic Nb_2O_5 nanocrystals from high temperature (700 °C) heat-treatment under N_2 atmosphere, but also improve the electrical conductivity of m-Nb_2O_5−C with enhanced electron transportation.[35] Here, we report an advanced HSC with an m-Nb_2O_5−C anode combined with an activated carbon (MSP-20) cathode. The novel HSC system described in this paper had superior electrochemical properties, including energy and power densities, because of the synergistic effects of the mesoporous structure and pseudocapacitive properties of Nb_2O_5.

RESULTS AND DISCUSSION

Synthesis of m-Nb_2O_5−C. Scheme 1 shows a schematic diagram of m-Nb_2O_5−C synthesis and a HSC system. The m-Nb_2O_5−C was synthesized by a one-pot synthesis method, which is evaporation-induced self-assembly (EISA), using niobium precursors and a laboratory-synthesized amphiphilic block copolymer (PEO-*b*-PS).[30] The niobium precursors undergo a non-hydrolytic sol−gel reaction to form a niobium oxide sol which interacts with the hydrophilic PEO block *via* hydrogen bonding, in an organic solvent. After an evaporation process for self-assembly, heat-treatment

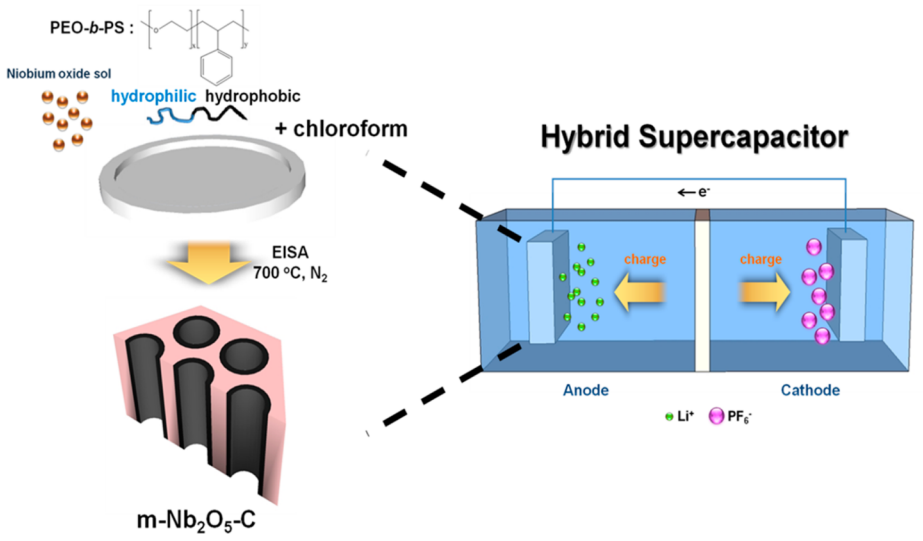

Scheme 1. Schematic diagram of one-pot synthesis of m-Nb_2O_5—C and hybrid supercapacitor system comprising m-Nb_2O_5—C anode and MSP-20 cathode.

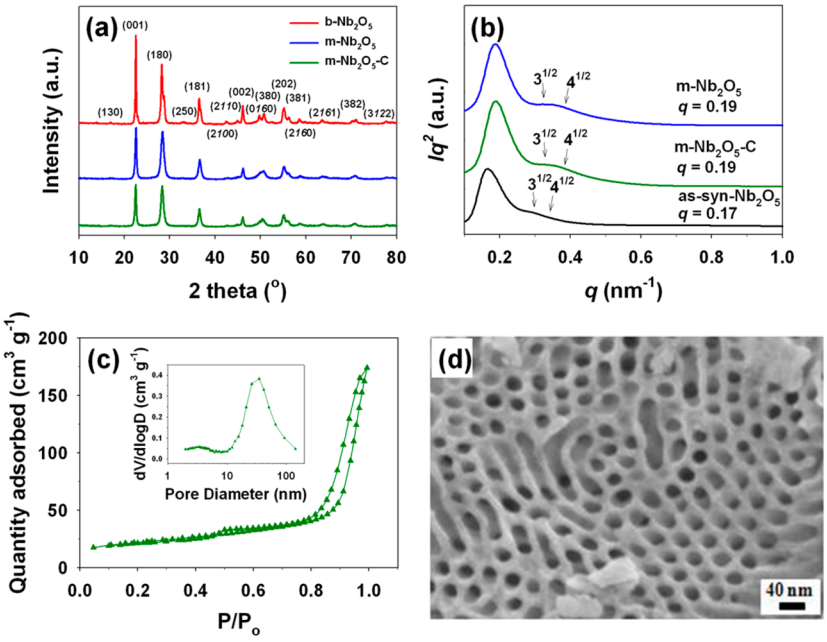

Figure 1. (a) XRD patterns of m-Nb_2O_5—C, m-Nb_2O_5, and b-Nb_2O_5. (b) SAXS traces of as-synthesized Nb_2O_5, m-Nb_2O_5—C, and m-Nb_2O_5. (c) N_2 adsorption—desorption isotherm for m-Nb_2O_5—C and the corresponding pore size distribution. (d) SEM image of m-Nb_2O_5—C.

of the niobium oxide sol/PEO-*b*-PS assembled composite at 700 °C under N_2 afforded highly ordered mesoporous structures. The resulting m-Nb_2O_5—C was used as the anode active material in the HSC system. For control experiments, mesoporous Nb_2O_5 (denoted by m-Nb_2O_5, obtained by m-Nb_2O_5—C heat-treatment in air) and nanometer-sized bulk Nb_2O_5 (denoted by b-Nb_2O_5, synthesized without a block copolymer) were prepared.

The X-ray diffraction (XRD) patterns of Nb_2O_5 samples (Figure 1a) match the orthorhombic phase (JCPDS No. 30-0873) of Nb_2O_5. The crystallite sizes of m-Nb_2O_5—C, m-Nb_2O_5, and b-Nb_2O_5, calculated using the Debye—Scherrer equation,[36] were 12, 12, and 21 nm, respectively. The crystallite sizes of m-Nb_2O_5—C and m-Nb_2O_5 were approximately half that of b-Nb_2O_5; the size was not changed during heat-treatment in air (m-Nb_2O_5—C to m-Nb_2O_5). As confirmed in previous studies, small crystallites favor Li^+ insertion into Nb_2O_5 electrodes, with an improved surface charge contribution.[23,33]

Small-angle X-ray scattering (SAXS) patterns show that the as-synthesized Nb_2O_5 (block copolymer/precursors composite annealed at 100 °C), m-Nb_2O_5—C, and m-Nb_2O_5 have long-range ordered structures (Figure 1b). The arrows in the figure represent the relative scattering vector (q) positions $3^{1/2}$ and $4^{1/2}$ from the first-order

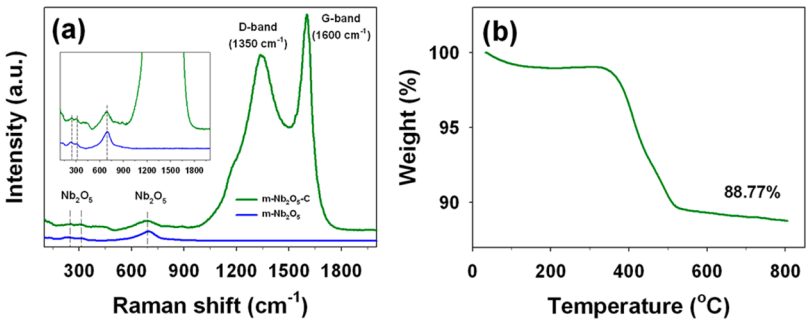

Figure 2. (a) Raman spectra of m-Nb_2O_5−C and m-Nb_2O_5 (580−740 cm^{-1}, Nb−O−Nb bridging bond of distorted NbO_6; 180−350 cm^{-1}, Nb−O−Nb angle deformation). (b) TGA profile of m-Nb_2O_5−C.

maximum, indicating that the hexagonally ordered Nb_2O_5 structure is well developed. The *q* value of as-synthesized Nb_2O_5 compared to that of m-Nb_2O_5−C and m-Nb_2O_5 was slightly larger (an increase from 0.17 to 0.19); this is attributed to framework shrinkage during heat-treatment. Notably, the SAXS pattern of m-Nb_2O_5 shows well preserved patterns compared to that of as-synthesized Nb_2O_5 and m-Nb_2O_5−C. It represents that the highly ordered mesostructure with high crystallinity was well developed by block copolymer assisted self-assembly.[30] The mesoporous structures of the Nb_2O_5 samples were further characterized using N_2 adsorption−desorption isotherms (Figure 1c) and scanning electron microscope (SEM; Figure 1d). The N_2 adsorption curves of mesoporous Nb_2O_5 materials exhibit type IV curves, with a sharp adsorption at ~0.9 P/P_o (Figure 1c and Figure S1a). This indicates extensive generation of uniform mesopores, in particular large pores that can be used as appropriate pathways for electrolyte penetration. The main pore size, calculated using the Barrett−Joyner−Halenda (BJH) method, and the Brunauer−Emmett−Teller (BET) surface area of m-Nb_2O_5−C were 30 nm and 76 $m^2\ g^{-1}$, respectively.[37] After removal of *in situ* formed carbon, the pore size and surface area were 50 nm and 40 $m^2\ g^{-1}$, respectively. The surface area of the mesostructured material was much higher than that of b-Nb_2O_5 (<3 $m^2\ g^{-1}$). It should be mentioned that the synthesis of mesoporous material (>30 nm) is only feasible when laboratory-synthesized PEO-*b*-PS with higher molecular weight and Flory-Huggins interaction parameter is used as a structure-directing agent,[38,39] which is not possible to synthesize using Pluronic-based commercial block copolymers. SEM images of m-Nb_2O_5−C, as-synthesized Nb_2O_5, and m-Nb_2O_5 (Figure 1d and Figure S1b, c) show uniformly generated mesopores with a well-ordered hexagonal array, consistent with the SAXS and the N_2 physisorption results.

Raman spectroscopy and thermogravimetric analysis (TGA) were employed to confirm the presence of *in situ* formed carbon of m-Nb_2O_5−C as shown in Figure 2. The presence of carbon in m-Nb_2O_5−C is verified by Raman spectroscopy with two bands around 1600 (graphitic carbon, G-band) and 1350 (disordered carbon, D-band) cm^{-1}, respectively.[30,40] TGA result is also in good agreement with the result of Raman spectroscopy, indicating the presence of *in situ* formed carbon where the carbon content is about 11 wt % as shown Figure 2b. Furthermore, electron energy loss spectroscopy (EELS) analysis image was used to directly confirm the existence of carbon in m-Nb_2O_5−C. Figure S2 clearly shows that the carbon-coated mesostructure is well synthesized. In this study, the *in situ* formed carbon plays key roles in not only maintaining the mesostructure from the high heat-treatment under N_2 atmosphere, but also improving electronic network in m-Nb_2O_5−C. When compared with the mesoporous Nb_2O_5 (main pore size: 13−15 nm) thin film prepared by KLE block copolymer, our method was based on block copolymer (PEO-*b*-PS) as a structure directing agent to produce the carbon-coated mesoporous Nb_2O_5 (~30 nm) powder comprising nanosized Nb_2O_5 particles (m-Nb_2O_5−C) *via* one-pot synthesis method without any further treatment.[41] Hence, it is expected that our m-Nb_2O_5−C material has several merits such as simple preparation with easy scale-up and lower cost.

Electrochemical characterization. *Nb_2O_5/Li and MSP-20/Li Half-Cell Test.* To investigate the electrochemical performance of Nb_2O_5 electrodes, half-cells were prepared using a 2032-type coin cell with lithium metal as the counter and reference electrodes. Cyclic voltammetry (CV) tests at sweep rates from 0.1 to 4.8 mV s^{-1} were conducted to examine the pseudocapacitive behavior of m-Nb_2O_5−C (Figure S3a,b).[19,23] The broad cathodic and anodic peaks in the potential ranges of 1.1−2.2 V from the CV data can be attributed to $Nb_2O_5 + xLi^+ + xe^- \leftrightarrow Li_xNb_2O_5$, where *x* is the degree of lithium insertion from 0 to 2.[42] Generally, the current (*i*) and sweep rates (*v*) have the relationship $i = av^b$ (*a* and *b* are appropriate values), obeying the power law.[43] It has been well established in previous studies that the *b* value in pseudocapacitive behavior is usually distinct from that in the case of the Li^+ intercalation process;[23,33] $b = 0.5$ represents a diffusion-controlled process caused by cation intercalation and $b = 1$ symbolizes capacitive behavior *via* a surface faradaic redox reaction.[23,43] As Figure 3a (and Figure S4a) shows, the relationships between *i* and *v* for m-Nb_2O_5−C

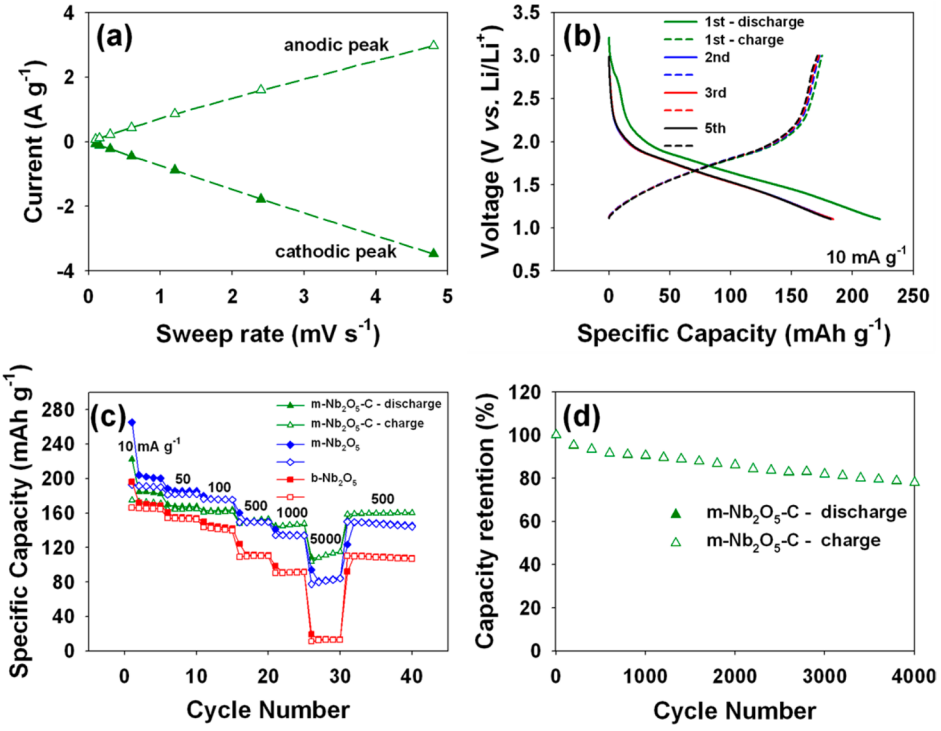

Figure 3. (a) Specific peak current of m-Nb_2O_5—C electrode for sweep rates ranging from 0.1 to 4.8 mV s^{-1}. (b) Charge—discharge profiles of m-Nb_2O_5—C at 10 mA g^{-1}. (c) Comparison of capacities of the Nb_2O_5/Li half-cells under different current densities varying from 10 to 5000 mA g^{-1}. (d) Cycling performance of m-Nb_2O_5—C at 2000 mA g^{-1} current density. Before cycling test, precycling (two cycles) was conducted at 40 mA g^{-1}. (b—d) Potential range was 1.1—3.0 V (*vs* Li/Li^+).

are linear (b = 1), suggesting that its charge-storage behavior is best described as pseudocapacitive behavior.[19,23,24,41] The CV measurements for different mass loadings (0.60—2.23 mg) of m-Nb_2O_5—C at sweep rates from 0.1 to 50 mV s^{-1} were also performed to additionally examine its pseudocapacitive property as shown in Figures S3 and S4b. From the relations between i and v, it should be noted that the charge-storage mechanism trend of m-Nb_2O_5—C is not changed with respect to various mass loadings of m-Nb_2O_5—C, mainly due to its unique electrochemical property. At high sweep rates, a small deviation of the high mass loading electrode is probably due to the high total internal resistances from the high loading, which is not resulted from the change of charging mechanism.[23]

The galvanostatic charge—discharge (delithiation—lithiation) voltage profiles over Nb_2O_5 electrodes at a current density of 10 mA g^{-1} in the potential window 1.1—3.0 V (*vs* Li/Li^+) are displayed in Figure 3b (and Figure S5a,b). The discharge capacities of m-Nb_2O_5 electrodes were larger than those of b-Nb_2O_5, indicating significant enhancement of electrochemical activity by the mesostructured Nb_2O_5. Furthermore, the charge—discharge profiles did not change significantly after the first cycle even though the first irreversible capacity losses of m-Nb_2O_5—C, m-Nb_2O_5, and b-Nb_2O_5 were 21.4, 27.3, and 15.3%, respectively. In general, nanostructured electrode materials have an irreversible capacity of approximately 20—40%.[44,45] Note that the capacity of m-Nb_2O_5—C electrode was smaller than that of m-Nb_2O_5 at low current densities (10—100 mA g^{-1}); this is caused by small capacity contribution of the *in situ* formed carbon (~11 wt %) in m-Nb_2O_5—C as shown in Figure S6. The real contribution of *in situ* formed carbon in m-Nb_2O_5—C for specific capacity may be approximately less than 2 mA h g^{-1}, considering low capacity of ordered mesoporous carbon (<20 mA h g^{-1}) and the carbon content (~11 wt %) in m-Nb_2O_5—C. Interestingly, the charge—discharge curves of the m-Nb_2O_5—C electrode exhibited more sloped patterns compared to that of $Li_4Ti_5O_{12}$ in the voltage range from 2.2 to 1.1 V, which is in good agreement with the broad cathodic—anodic peaks in the CV results (Figure S3). When compared with the voltage plateau at ~1.55 V in $Li_4Ti_5O_{12}$ electrode, furthermore, the inclined trend of charge—discharge profiles in m-Nb_2O_5—C electrode can lead to better prediction of state-of-charge (SOC), which is highly beneficial in high power application.

Figure 3c shows the rate performances of m-Nb_2O_5—C, m-Nb_2O_5, and b-Nb_2O_5 electrodes for various current densities from 10 to 5000 mA g^{-1} in the voltage window of 1.1—3.0 V (*vs* Li/Li^+). The charge—discharge capacities and capacity retentions of the mesostructured Nb_2O_5 electrodes were much higher than those of the b-Nb_2O_5 electrode at all current densities. This shows that the mesoporous structure improves the rate capability, mainly because of improved electrolyte penetration through the mesopores and shortened Li^+ diffusion

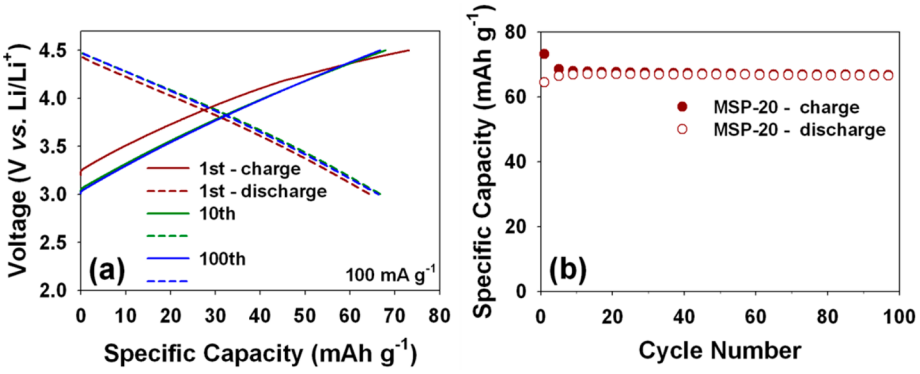

Figure 4. (a) Charge−discharge profiles of MSP-20. (b) Cycling performance of the MSP-20 at 100 mA g^{-1} between 3.0 and 4.5 V (*vs* Li/Li^+).

lengths within the pore walls.[41,46] A more developed pseudocapacitive contribution in the nanocrystal surface (12 nm) could also be a reason for the improved rate capability.[33] As shown in Figure S4a, the *b* values of the m-Nb_2O_5−C and m-Nb_2O_5 electrodes were very close to 1, but large deviation from 1 were observed for the b-Nb_2O_5 electrode, which again indicates that the introduction of porous structure comprising nanosized Nb_2O_5 nanocrystals improves kinetics in electrochemical reactions. In previous studies, it was reported that the charge-storage mechanism is changed from the diffusion-limited Li^+ intercalation process to surface faradaic reactions in the nanosized materials.[33,47] In particular, the charge−discharge capacity of m-Nb_2O_5−C (115.1 mA h g^{-1}) was far higher than that of m-Nb_2O_5 (84.4 mA h g^{-1}) and b-Nb_2O_5 (12.9 mA h g^{-1}) at very high current density (5000 mA g^{-1}, equivalent to 25 C rate); this might be one of the best rate performances ever reported for titanium or niobium oxide-based anode materials.[46,48] The excellent rate performance of m-Nb_2O_5−C is clearly shown in Figure S7a−c. The charge−discharge profiles under different current densities show that an improved rate performance of m-Nb_2O_5−C compared with that of the others was observed with increasing current density. Clearly, the high rate performance of the m-Nb_2O_5−C electrode compared with that of m-Nb_2O_5 is attributable to enhanced electrical conductivity owing to the presence of conductive carbon derived from the PS-block. As summarized in Table S1, the electrical conductivity of m-Nb_2O_5−C is much higher than that of m-Nb_2O_5 and pure Nb_2O_5 previously reported.[28] In other words, the carbon layer in m-Nb_2O_5−C provides a fast electronic conduction into insulating Nb_2O_5 nanocrystals, resulting in a reduced internal resistance of Nb_2O_5 electrode. Therefore, this promoted electron supply through the *in situ* carbon gives rise to a fast response at high current density (at 5000 mA g^{-1}) by maintaining the pseudocapacitive reaction of Nb_2O_5.

Figure 3d shows the cycling performance of the m-Nb_2O_5−C/Li half cell at a current rate of 2000 mA g^{-1}. During prolonged cycling (4000 cycles), ~80% of the initial capacity is retained, *i.e.*, much higher stability than that of other intercalation-based Li^+ insertion materials is achieved.[18,46,49] The cycling stability might be attributed to the unique structure of m-Nb_2O_5−C, which is a uniformly carbon-coated mesostructure. As reported by previous study, amorphous carbon layer on electrode materials has resulted in suppressed surface side reaction during cycling.[50] In this study, the *in situ* formed carbon in m-Nb_2O_5−C could play an important role in enhancing the surface stability of Nb_2O_5. In the HSC system, electric double-layer type cathodes such as activated and porous carbon electrodes are typically used, which conventionally exhibit much better rate performances and more stable cycle life than battery type anodes. Therefore, the m-Nb_2O_5−C electrode is the most suitable anode for HSC performance improvement, because of its significantly improved rate capability and extended cycling lifetime. Before constructing the HSC, the MSP-20 electrode was also tested in a half-cell at a current rate of 100 mA g^{-1} in the voltage window 3.0−4.5 V (Figure 4). The charge−discharge profiles of the MSP-20 electrode do not significantly change during repeated cycles, with an acceptably high capacity of ~70 mA h g^{-1}.[18] The characteristic linear profiles reveal that the MSP-20 electrode operates *via* nonfaradaic capacitive reactions, in which ions are adsorbed and desorbed on the surface.[51]

Nb_2O_5//MSP-20 Hybrid Supercapacitor Test. To achieve the high-energy and -power densities of HSCs, the mass ratio of the electrodes was optimized as shown in Figure S8a. The best mass ratio of cathode and anode active materials was carefully balanced to 3:1 in the voltage range of 0.5−3.0 V for high electrochemical performances of the HSCs. CV was performed to evaluate the electrochemical properties of the HSC in the voltage range 0.5−3.0 V at various scan rates from 2 to 50 mV s^{-1} (Figure 5). Because of the negligible capacity achieved less than 0.5 V in the HSC, the cutoff voltage was limited to 0.5 V. In this respect, we first optimize the HSC full cells in the voltage window between 0.5 and 3.0 V. In contrast to symmetric SCs with rectangular CV profiles, our HSC

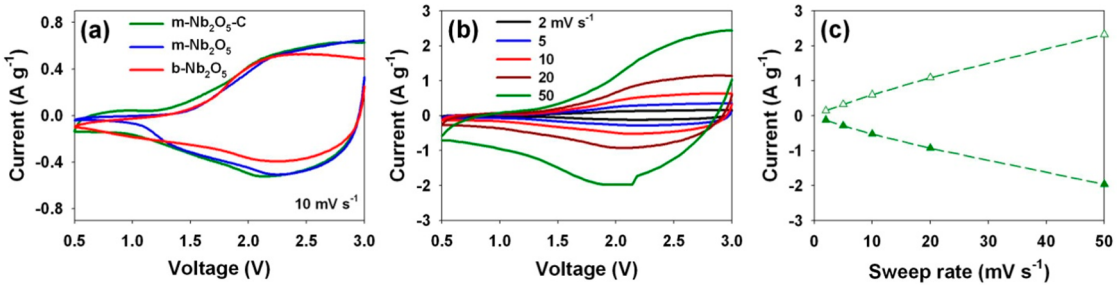

Figure 5. (a) CV curves of hybrid supercapacitors based on m-Nb_2O_5—C, m-Nb_2O_5, and b-Nb_2O_5 anodes at a scan rate of 10 mV s^{-1}. (b) CV curves of hybrid supercapacitor using m-Nb_2O_5—C anode at various scan rates from 2 to 50 mV s^{-1}. (c) Specific peak current of hybrid supercapacitor based on m-Nb_2O_5—C anode with respect to various sweep rates from 2 to 50 mV s^{-1}.

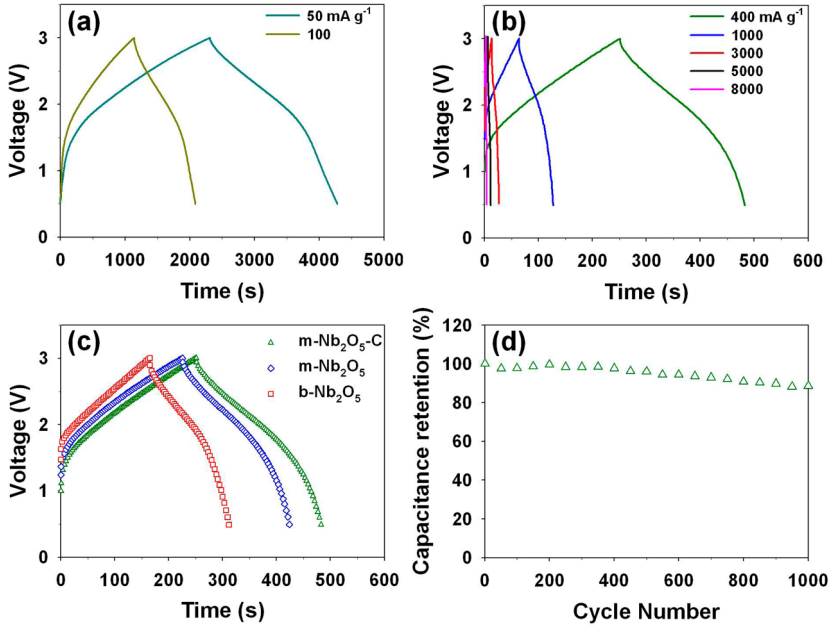

Figure 6. (a and b) Charge—discharge profiles of hybrid supercapacitor based on m-Nb_2O_5—C anode at different current rates. (c) Charge—discharge profiles of hybrid supercapacitors at 400 mA g^{-1}. (d) Cycling performance of hybrid supercapacitor based on m-Nb_2O_5—C anode at a current rate of 1000 mA g^{-1}.

has an asymmetric CV profile, indicating introduction of a faradaic reaction into the HSC system.[18,52] The intrinsic redox active property of Nb_2O_5 anode materials may contribute to the asymmetric CV profile with deviation from the quasi-broad rectangular CV. In the CV analysis, the cathodic and anodic currents of the HSC based on m-Nb_2O_5—C increased compared to the HSCs with m-Nb_2O_5 and b-Nb_2O_5 anodes, while maintaining the curve shapes, showing that the electrochemical activity of the HSC with the m-Nb_2O_5—C anode is higher than those of the control groups. In addition, the linear relationship between current response peaks and scan rates, shown in Figure 5c, reveals that the charge-storage reaction in the HSC is mainly based on surface faradaic reactions rather than diffusion-limited reactions.[12] The electrochemical properties of the HSCs based on the m-Nb_2O_5—C electrode anode were further investigated by galvanostatic measurements at current rates from 50 to 8000 mA g^{-1}, as shown in Figure 6a,b. The charge—discharge profiles of the HSC were not typical triangular shapes, unlike those of symmetric SCs.[52] This again shows that the charge-storage mechanism in the HSC is based on a combination of a faradaic pseudocapacitive reaction at the anode and nonfaradaic capacitive charge-storage at the cathode. The charge—discharge curves of the HSC using m-Nb_2O_5—C were measured and compared with those of the HSCs using m-Nb_2O_5 and b-Nb_2O_5 at 400 mA g^{-1} as shown in Figure 6c. The charge—discharge time of the HSC using an m-Nb_2O_5—C anode was much longer than those of the HSCs using m-Nb_2O_5 and b-Nb_2O_5 at a current rate of 400 mA g^{-1}, again indicating the electrochemical performance of the HSC with m-Nb_2O_5—C anode is superior compared to those of the control groups. Furthermore, the HSC using m-Nb_2O_5—C shows stable cyclability over 1000 cycles (~90%) without noticeable capacity fading as shown in Figure 6d.

Figure 7 shows a Ragone plot representing the trade-off between power and energy density, which

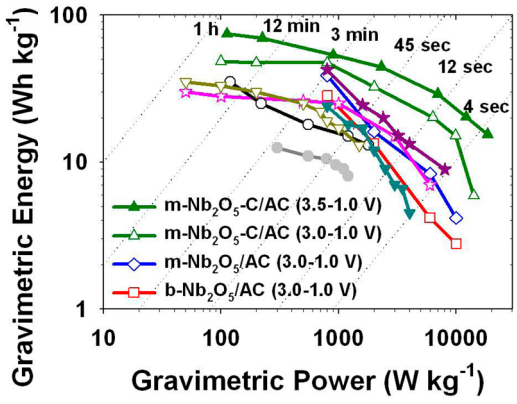

Figure 7. Ragone plots of hybrid supercapacitors based on m-Nb_2O_5—C, m-Nb_2O_5, and b-Nb_2O_5 anodes. The energy and power densities were compared with other hybrid supercapacitor systems using anatase TiO_2//AC (★),[18] CNT/Nb_2O_5//AC (☆),[29] $LiCrTiO_4$//AC (▼),[55] C—$Li_4Ti_5O_{12}$//AC (▽),[54] $Li_{1.2}(Mn_{0.32}Ni_{0.32}Fe_{0.16})O_2$//AC (○),[56] TiO_2(B)//CNT (●).[11]

is important for practical applications. The Ragone plot was calculated using galvanostatic measurements (Figure 6a,b). The power and energy densities were calculated by numerically integrating the galvanostatic discharge curves as follows:[18,19,53]

$$E = \int_{t_1}^{t_2} IV\,dt = \frac{1}{2}C(E_{max} + E_{min})(E_{max} - E_{min}) = \Delta V \times \frac{I}{m} \times t \quad (1)$$

$$P = \frac{E}{t} = \Delta V \times \frac{I}{m} \quad (2)$$

$$\Delta V = \frac{E_{max} + E_{min}}{2} \quad (3)$$

where C (= $[(I \times t)/m] \times [1/(E_{max} - E_{min})]$) is the specific capacitance (F g^{-1}), E_{max} (3.0 or 3.5 V) and E_{min} (1.0 V) are the initial and final discharge potentials (V), I is the discharge current (A), t is the discharge time (s), and m is the total mass of active materials in both anode and cathode.

The performance of the HSC using m-Nb_2O_5—C significantly surpasses that of the control group. In addition, the Ragone plot shows that the specific power and energy densities of the HSC using m-Nb_2O_5—C is higher compared to similar HSC systems including TiO_2(B)//CNT (●), C—$Li_4Ti_5O_{12}$//AC (▽), anatase TiO_2//AC (★), CNT/Nb_2O_5//AC (☆), $LiCrTiO_4$//AC (▼), and $Li_{1.2}(Mn_{0.32}Ni_{0.32}Fe_{0.16})O_2$//AC (○).[11,18,29,54−56] The maximum energy and power densities of this system were 48 W h kg^{-1} and 14 164 W kg^{-1}, respectively. The high energy density of ~15 W h kg^{-1} was maintained at a 5.5 s discharge rate, delivering 9897 W kg^{-1}, which is better performance compared with other similar HSC systems. To maximize energy and power densities, the cutoff voltage at the end of charging was increased to 3.5 V (Figure S9a,b). In the best mass ratio (2.5:1) of cathode and anode active materials (Figure S8b), the maximum energy (74 W h kg^{-1}) and power (18 510 W kg^{-1}) densities were achieved, respectively, without significant capacity degradation (Figure S9c). Furthermore, a high energy density of 20 W h kg^{-1} was achieved at a 6 s discharge rate with 12 137 W kg^{-1}. Even at 15 W h kg^{-1}, the highest power density of 18 510 W kg^{-1} was achieved, demonstrating that the HSC using m-Nb_2O_5—C covers the wide energy and power density regions. This is particularly important for HSCs to bridge between LIBs and SCs, because it is generally not easy for LIBs and SCs to achieve such high energy density at high power region. As shown in Figure S10, the HSC system would be recognized as a next-generation energy-storage device, mainly because of its exceptional electrochemical performances. The reasons for the outstanding electrochemical properties of the HSC using m-Nb_2O_5—C are as follows. (i) Li^+ charge storage preferentially happens in outer surface of Nb_2O_5 rather than Li-intercalation reaction accompanied by slow solid-state diffusion.[23,24] (ii) The porous structure improves surface redox reactions *via* a large electrolyte-electrode interface area.[32,57] (iii) The interconnected mesoporous structure can provide enhanced ion transport.[32] (iv) The *in situ* formed carbon significantly increases the electrical conductivity throughout the electrode.[46]

CONCLUSIONS

In conclusion, the electrochemical performances of Nb_2O_5 electrodes synthesized by a one-pot synthesis method were solidly investigated for use in HSC systems. The results revealed that the synthesized Nb_2O_5 samples showed high capacities and rate properties, mainly because of their pseudocapacitive properties. In particular, a novel HSC system comprising a m-Nb_2O_5—C nanocomposite anode with an MSP-20 cathode provided superior energy and power densities (74 W h kg^{-1} and 18 510 W kg^{-1}), with excellent cycling stability. The performance of the HSC using m-Nb_2O_5—C is comparable or even higher than that of other HSC systems reported. In particular, the highest power density (18 510 W kg^{-1}) of the HSC using m-Nb_2O_5—C was achieved at 15 W h kg^{-1}, which is a remarkable result compared to other similar HSC systems. With more research, this HSC system could be one of the main energy-storage systems, along with conventional LIBs and SCs.

METHODS

Synthesis of Nb_2O_5 Samples. The m-Nb_2O_5—C and m-Nb_2O_5 were synthesized by a simple one-pot method using block copolymer (PEO-*b*-PS, M_n = 40 700 g/mol, and 12.9 wt % of PEO). For the synthesis of m-Nb_2O_5—C, niobium ethoxide (0.19 mL, 0.75 mmol) and niobium chloride (0.20 g, 0.75 mmol) were

stirred together in 20 mL of chloroform with 0.2 g of PEO-*b*-PS. The solution was stirred for 5 h at room temperature and then poured onto a Petri-dish. The Petri-dish was heated to 50 °C to obtain the as-synthesized transparent film. The as-synthesized transparent film was dried at 100 °C overnight and carefully collected. The collected resulting material was heat-treated in N_2 condition at 700 °C for 2 h. To obtain m-Nb_2O_5, the *in situ* formed carbon of m-Nb_2O_5−C was removed by subsequent calcination in air at 450 °C for 2 h. The b-Nb_2O_5 was also prepared by same method mentioned above without PEO-*b*-PS.

Characterization of Nb_2O_5 Samples. The Bruker D8 Advance X-ray diffractometer (Cu Kα radiation) was employed for identifying powder XRD patterns. Thermogravimetric analysis (TGA) was performed on a NETZSCH STA 449C thermobalance. SAXS patterns were identified using 4C SAXS beamline at the Pohang Light Source (PLS). The nitrogen adsorption−desorption experiments were conducted using a Tristar II 3020 instrument (Micromeritics Instrument Corporation). The mesoporous structures were confirmed by SEM with an S-4200 field-emission SEM (Hitachi). The electron energy loss spectroscopy analysis was carried out using energy-filtering transmission electron microscopy (EF-TEM, JM-220FS). For the TEM analysis, the m-Nb_2O_5−C sample was sectioned at a thickness of 100 nm using a SIMS powertome XL. A Raman spectrometer (Horiba Jobin Yvon, LabRam Aramis) was employed with a laser at 514.532 nm (Ar-ion laser) at a power of 100 uW.

Electrochemical Characterization. For the preparation of anode of half-cell tests, the active materials (80 wt %), super-P carbon (10 wt %) and polyvinylidene fluoride (PVDF) (10 wt %) were homogeneously mixed in *N*-methyl-2-pyrrolidone (NMP), and then the mixtures were coated on a piece of Cu foil. The electrodes were dried at 110 °C overnight and then roll-pressed. The 2032-type coin cells with a Li metal were assembled in Ar-filled glovebox. $LiPF_6$ (1.0 M) in a mixture of ethylene carbonate (EC) and dimethyl carbonate (DMC) was used as the electrolyte (EC/DMC, 1:1 volume ratio, Panaxetec Co., Korea). For the charge−discharge test of Nb_2O_5 samples, the mass loading of active materials was controlled approximately by 0.4−1.4 mg cm^{-2}. For cathode of half-cell tests, an activated carbon (MSP-20, 90 wt %) with conductive carbon (5 wt %) and polytetrafluoroethylene (PTFE, 5 wt %) were mixed together, and then the cathode cell was assembled by the same method mentioned above. For full-cell tests of the hybrid supercapacitors, the full-cells were assembled using both Nb_2O_5 electrodes as an anode and MSP-20 as a cathode. The counter references including m-Nb_2O_5 and b-Nb_2O_5 were also assembled. Additionally, the weight ratio of cathode and anode active materials was carefully balanced to 3:1 in the voltage range of 0.5−3.0 V and 2.5:1 in that of 0.5−3.5 V to deliver optimized electrochemical performances.

Conflict of Interest: The authors declare no competing financial interest.

Supporting Information Available: The further characterization of Nb_2O_5 samples such as BET, SEM, and electrochemical data (cyclic voltammetry, galvanostatic charge−discharge curves, *etc.*). This material is available free of charge *via* the Internet at http://pubs.acs.org.

Acknowledgment. This work was supported by the Global Frontier R&D Program on Center for Multiscale Energy System under the Ministry of Education, Basic Science Research Program (NRF-2013R1A1A2074550), and (No. 2012R1A2A2A01002879) by the Ministry of Science, ICT and Future Planning funded by the National Research Foundation (NRF). This work was further supported by Defense Acquisition Program Administration and Agency for Defense Development under the contract UD 110090GD, a grant of the Korea Health 21 R&D Project of Ministry of Health & Welfare (A121631). This research was a part of the project titled 'Technology Development of Marine Industrial Biomaterials' funded by the Ministry of Oceans and Fisheries, Korea. This research was supported by the MSIP (Ministry of Science, ICT and Future Planning), Korea, under the "IT Consilience Creative Program" (NIPA-2014-H0201-14-1001) supervised by the NIPA (National IT Industry Promotion Agency). This work was supported by the Human Resources Development program (20124010203320) of the Korea Institute of Energy Technology Evaluation and Planning (KETEP) grant funded by the Korea government Ministry of Trade, Industry and Energy.

REFERENCES AND NOTES

1. Kang, K.; Meng, Y. S.; Bréger, J.; Grey, C. P.; Ceder, G. Electrodes with High Power and High Capacity for Rechargeable Lithium Batteries. *Science* **2006**, *311*, 977–980.
2. Chiang, Y.-M. Building a Better Battery. *Science* **2010**, *330*, 1485–1486.
3. Poizot, P.; Laruelle, S.; Grugeon, S.; Dupont, L.; Tarascon, J. M. Nano-Sized Transition-Metal Oxides as Negative-Electrode Materials for Lithium-Ion Batteries. *Nature* **2000**, *407*, 496–499.
4. Simon, P.; Gogotsi, Y. Materials for Electrochemical Capacitors. *Nat. Mater.* **2008**, *7*, 845–854.
5. Taberna, P.-L.; Mitra, S.; Poizot, P.; Simon, P.; Tarascon, J.-M. High Rate Capabilities Fe_3O_4-Based Cu Nano-Architectured Electrodes for Lithium-Ion Battery Applications. *Nat. Mater.* **2006**, *5*, 567–573.
6. Lee, J. E.; Yu, S.-H.; Lee, D. J.; Lee, D.-C.; Han, S. I.; Sung, Y.-E.; Hyeon, T. Facile and Economical Synthesis of Hierarchical Carbon-Coated Magnetite Nanocomposite Particles and Their Applications in Lithium Ion Battery Anodes. *Energy Environ. Sci.* **2012**, *5*, 9528–9533.
7. Yuan, F.-W.; Yang, H.-J.; Tuan, H.-Y. Alkanethiol-Passivated Ge Nanowires as High-Performance Anode Materials for Lithium-Ion Batteries: The Role of Chemical Surface Functionalization. *ACS Nano* **2012**, *6*, 9932–9942.
8. Lee, K. T.; Jung, Y. S.; Oh, S. M. Synthesis of Tin-Encapsulated Spherical Hollow Carbon for Anode Material in Lithium Secondary Batteries. *J. Am. Chem. Soc.* **2003**, *125*, 5652–5653.
9. Balke, N.; Jesse, S.; Morozovska, A. N.; Eliseev, E.; Chung, D. W.; Kim, Y.; Adamczyk, L.; Garcia, R. E.; Dudney, N.; Kalinin, S. V. Nanoscale Mapping of Ion Diffusion in a Lithium-Ion Battery Cathode. *Nat. Nanotechnol* **2010**, *5*, 749–754.
10. Lee, S. H.; Yu, S.-H.; Lee, J. E.; Jin, A.; Lee, D. J.; Lee, N.; Jo, H.; Shin, K.; Ahn, T.-Y.; Kim, Y.-W.; *et al.* T. Self-Assembled Fe_3O_4 Nanoparticle Clusters as High-Performance Anodes for Lithium Ion Batteries *via* Geometric Confinement. *Nano Lett.* **2013**, *13*, 4249–4256.
11. Wang, Q.; Wen, Z. H.; Li, J. H. A Hybrid Supercapacitor Fabricated with a Carbon Nanotube Cathode and a TiO_2-B Nanowire Anode. *Adv. Funct. Mater.* **2006**, *16*, 2141–2146.
12. Lee, S. W.; Yabuuchi, N.; Gallant, B. M.; Chen, S.; Kim, B.-S.; Hammond, P. T.; Shao-Horn, Y. High-Power Lithium Batteries from Functionalized Carbon-Nanotube Electrodes. *Nat. Nanotechnol.* **2010**, *5*, 531–537.
13. Naoi, K.; Naoi, W.; Aoyagi, S.; Miyamoto, J.-i.; Kamino, T. New Generation "Nanohybrid Supercapacitor. *Acc. Chem. Res.* **2012**, *46*, 1075–1083.
14. Naoi, K.; Ishimoto, S.; Miyamoto, J.-i.; Naoi, W. Second Generation 'Nanohybrid Supercapacitor': Evolution of Capacitive Energy Storage Devices. *Energy Environ. Sci.* **2012**, *5*, 9363–9373.
15. Cheng, L.; Liu, H.-J.; Zhang, J.-J.; Xiong, H.-M.; Xia, Y.-Y. Nanosized $Li_4Ti_5O_{12}$ Prepared by Molten Salt Method as an Electrode Material for Hybrid Electrochemical Supercapacitors. *J. Electrochem. Soc.* **2006**, *153*, A1472–A1477.
16. Chen, Z.; Augustyn, V.; Wen, J.; Zhang, Y.; Shen, M.; Dunn, B.; Lu, Y. High-Performance Supercapacitors Based on Intertwined CNT/V_2O_5 Nanowire Nanocomposites. *Adv. Mater.* **2011**, *23*, 791–795.
17. Naoi, K. 'Nanohybrid Capacitor': The Next Generation Electrochemical Capacitors. *Fuel Cells* **2010**, *10*, 825–833.
18. Kim, H.; Cho, M.-Y.; Kim, M.-H.; Park, K.-Y.; Gwon, H.; Lee, Y.; Roh, K. C.; Kang, K. A Novel High-Energy Hybrid Supercapacitor with an Anatase TiO_2-Reduced Graphene Oxide Anode and an Activated Carbon Cathode. *Adv. Energy Mater.* **2013**, *3*, 1500–1506.

19. Wang, Y.; Hong, Z.; Wei, M.; Xia, Y. Layered $H_2Ti_6O_{13}$-Nanowires: A New Promising Pseudocapacitive Material in Non-Aqueous Electrolyte. *Adv. Funct. Mater.* **2012**, *22*, 5185–5193.
20. Naoi, K.; Ishimoto, S.; Isobe, Y.; Aoyagi, S. High-Rate Nano-Crystalline $Li_4Ti_5O_{12}$ Attached on Carbon Nano-Fibers for Hybrid Supercapacitors. *J. Power Sources* **2010**, *195*, 6250–6254.
21. Tarascon, J. M.; Armand, M. Issues and Challenges Facing Rechargeable Lithium Batteries. *Nature* **2001**, *414*, 359–367.
22. Kim, H.; Park, K. Y.; Cho, M. Y.; Kim, M. H.; Hong, J.; Jung, S. K.; Roh, K. C.; Kang, K. High-Performance Hybrid Supercapacitor Based on Graphene-Wrapped $Li_4Ti_5O_{12}$ and Activated Carbon. *ChemElectroChem* **2014**, *1*, 125–130.
23. Augustyn, V.; Come, J.; Lowe, M. A.; Kim, J. W.; Taberna, P.-L.; Tolbert, S. H.; Abruña, H. D.; Simon, P.; Dunn, B. High-Rate Electrochemical Energy Storage through Li^+ Intercalation Pseudocapacitance. *Nat. Mater.* **2013**, *12*, 518–522.
24. Kim, J. W.; Augustyn, V.; Dunn, B. The Effect of Crystallinity on the Rapid Pseudocapacitive Response of Nb_2O_5. *Adv. Energy Mater.* **2012**, *2*, 141–148.
25. Kang, S.-H.; Abraham, D. P.; Yoon, W.-S.; Nam, K.-W.; Yang, X.-Q. First-Cycle Irreversibility of Layered Li-Ni-Co-Mn Oxide Cathode in Li-ion Batteries. *Electrochim. Acta* **2008**, *54*, 684–689.
26. Han, J.-T.; Liu, D.-Q.; Song, S.-H.; Kim, Y.; Goodenough, J. B. Lithium Ion Intercalation Performance of Niobium Oxides: KNb_5O_{13} and $K_6Nb_{10.8}O_{30}$. *Chem. Mater.* **2009**, *21*, 4753–4755.
27. Wei, M.; Wei, K.; Ichihara, M.; Zhou, H. Nb_2O_5 nanobelts: A Lithium Intercalation Host with Large Capacity and High Rate Capability. *Electrochem. Commun.* **2008**, *10*, 980–983.
28. Viet, A. L.; Reddy, M. V.; Jose, R.; Chowdari, B. V. R.; Ramakrishna, S. Nanostructured Nb_2O_5 Polymorphs by Electrospinning for Rechargeable Lithium Batteries. *J. Phys. Chem. C* **2009**, *114*, 664–671.
29. Wang, X.; Li, G.; Chen, Z.; Augustyn, V.; Ma, X.; Wang, G.; Dunn, B.; Lu, Y. High-Performance Supercapacitors Based on Nanocomposites of Nb_2O_5 Nanocrystals and Carbon Nanotubes. *Adv. Energy Mater.* **2011**, *1*, 1089–1093.
30. Lee, J.; Christopher Orilall, M.; Warren, S. C.; Kamperman, M.; DiSalvo, F. J.; Wiesner, U. Direct Access to Thermally Stable and Highly Crystalline Mesoporous Transition-Metal Oxides with Uniform Pores. *Nat. Mater.* **2008**, *7*, 222–228.
31. Hwang, J.; Woo, S. H.; Shim, J.; Jo, C.; Lee, K. T.; Lee, J. One-Pot Synthesis of Tin-Embedded Carbon/Silica Nanocomposites for Anode Materials in Lithium-Ion Batteries. *ACS Nano* **2013**, *7*, 1036–1044.
32. Ye, Y.; Jo, C.; Jeong, I.; Lee, J. Functional Mesoporous Materials for Energy Applications: Solar cells, Fuel cells, and Batteries. *Nanoscale* **2013**, *5*, 4584–4605.
33. Wang, J.; Polleux, J.; Lim, J.; Dunn, B. Pseudocapacitive Contributions to Electrochemical Energy Storage in TiO_2 (Anatase) Nanoparticles. *J. Phys. Chem. C* **2007**, *111*, 14925–14931.
34. Abel, P. R.; Chockla, A. M.; Lin, Y.-M.; Holmberg, V. C.; Harris, J. T.; Korgel, B. A.; Heller, A.; Mullins, C. B. Nanostructured $Si_{(1-x)}Ge_x$ for Tunable Thin Film Lithium-Ion Battery Anodes. *ACS Nano* **2013**, *7*, 2249–2257.
35. Zhang, L.; Zhang, G.; Wu, H. B.; Yu, L.; Lou, X. W. Hierarchical Tubular Structures Constructed by Carbon-Coated SnO_2 Nanoplates for Highly Reversible Lithium Storage. *Adv. Mater.* **2013**, *25*, 2589–2593.
36. Krawitz, A. D. *Introduction to Diffraction in Materials Science and Engineering*; Wiley: New York, 2001; p 168.
37. Barrett, E. P.; Joyner, L. G.; Halenda, P. P. The Determination of Pore Volume and Area Distributions in Porous Substances. I. Computations from Nitrogen Isotherms. *J. Am. Chem. Soc.* **1951**, *73*, 373–380.
38. Shim, J.; Lee, J.; Ye, Y.; Hwang, J.; Kim, S.-K.; Lim, T.-H.; Wiesner, U.; Lee, J. One-Pot Synthesis of Intermetallic Electrocatalysts in Ordered, Large-Pore Mesoporous Carbon/Silica toward Formic Acid Oxidation. *ACS Nano* **2012**, *6*, 6870–6881.
39. Ramasamy, E.; Jo, C.; Anthonysamy, A.; Jeong, I.; Kim, J. K.; Lee, J. Soft-Template Simple Synthesis of Ordered Mesoporous Titanium Nitride-Carbon Nanocomposite for High Performance Dye-Sensitized Solar Cell Counter Electrodes. *Chem. Mater.* **2012**, *24*, 1575–1582.
40. Liang, C.; Hong, K.; Guiochon, G. A.; Mays, J. W.; Dai, S. Synthesis of a Large-Scale Highly Ordered Porous Carbon Film by Self-Assembly of Block Copolymers. *Angew. Chem. Int. Edn* **2004**, *43*, 5785–5789.
41. Brezesinski, K.; Wang, J.; Haetge, J.; Reitz, C.; Steinmueller, S. O.; Tolbert, S. H.; Smarsly, B. M.; Dunn, B.; Brezesinski, T. Pseudocapacitive Contributions to Charge Storage in Highly Ordered Mesoporous Group V Transition Metal Oxides with Iso-Oriented Layered Nanocrystalline Domains. *J. Am. Chem. Soc.* **2010**, *132*, 6982–6990.
42. Ohzuku, T.; Sawai, K.; Hirai, T. Electrochemistry of L-Niobium Pentoxide a Lithium/Non-Aqueous Cell. *J. Power Sources* **1987**, *19*, 287–299.
43. Lindström, H.; Södergren, S.; Solbrand, A.; Rensmo, H.; Hjelm, J.; Hagfeldt, A.; Lindquist, S.-E. Li^+ Ion Insertion in TiO_2 (Anatase). 2. Voltammetry on Nanoporous Films. *J. Phys. Chem. B* **1997**, *101*, 7717–7722.
44. Kim, G.; Jo, C.; Kim, W.; Chun, J.; Yoon, S.; Lee, J.; Choi, W. TiO_2 Nanodisks Designed for Li-Ion Batteries: A Novel Strategy for Obtaining an Ultrathin and High Surface Area Anode Material at the Ice Interface. *Energy Environ. Sci.* **2013**, *6*, 2932–2938.
45. Wang, J.; Bai, Y.; Wu, M.; Yin, J.; Zhang, W. Preparation and Electrochemical Properties of TiO_2 Hollow Spheres as an Anode Material for Lithium-Ion Batteries. *J. Power Sources* **2009**, *191*, 614–618.
46. Kang, E.; Jung, Y. S.; Kim, G.-H.; Chun, J.; Wiesner, U.; Dillon, A. C.; Kim, J. K.; Lee, J. Highly Improved Rate Capability for a Lithium-Ion Battery Nano-$Li_4Ti_5O_{12}$ Negative Electrode *via* Carbon-Coated Mesoporous Uniform Pores with a Simple Self-Assembly Method. *Adv. Funct. Mater.* **2011**, *21*, 4349–4357.
47. Brezesinski, T.; Wang, J.; Tolbert, S. H.; Dunn, B. Next Generation Pseudocapacitor Materials from Sol-Gel Derived Transition Metal Oxides. *J. Sol-gel Sci. Technol.* **2011**, *57*, 330–335.
48. Hao, S.; Xiao, X.; Hu, Z.; Sun, L.; Han, S.; Chen, D.; Liu, X. Improving the Electrochemical Performance of $Li_4Ti_5O_{12}$ Anode through Confinement into Ordered Bimodal Porous Carbon Frameworks. *J. Phys. Chem. C* **2013**, *117*, 26889–26895.
49. Jung, H.-G.; Myung, S.-T.; Yoon, C. S.; Son, S.-B.; Oh, K. H.; Amine, K.; Scrosati, B.; Sun, Y.-K. Microscale Spherical Carbon-Coated $Li_4Ti_5O_{12}$ as Ultra High Power Anode Material for Lithium Batteries. *Energy Environ. Sci.* **2011**, *4*, 1345–1351.
50. Zhao, L.; Hu, Y. S.; Li, H.; Wang, Z.; Chen, L. Porous $Li_4Ti_5O_{12}$ Coated with N-Doped Carbon from Ionic Liquids for Li-Ion Batteries. *Adv. Mater.* **2011**, *23*, 1385–1388.
51. Aravindan, V.; Cheah, Y. L.; Mak, W. F.; Wee, G.; Chowdari, B. V. R.; Madhavi, S. Fabrication of High Energy-Density Hybrid Supercapacitors Using Electrospun V_2O_5 Nanofibers with a Self-Supported Carbon Nanotube Network. *ChemPlusChem* **2012**, *77*, 570–575.
52. Karthikeyan, K.; Amaresh, S.; Aravindan, V.; Kim, H.; Kang, K. S.; Lee, Y. S. Unveiling Organic-Inorganic Hybrids as a Cathode Material for High Performance Lithium-Ion Capacitors. *J. Mater. Chem. A* **2013**, *1*, 707–714.
53. Aravindan, V.; Chuiling, W.; Reddy, M. V.; Rao, G. V. S.; Chowdari, B. V. R.; Madhavi, S. Carbon Coated Nano-$LiTi_2(PO_4)_3$ Electrodes for Non-Aqueous Hybrid Supercapacitors. *Phys. Chem. Chem. Phys.* **2012**, *14*, 5808–5814.
54. Jung, H.-G.; Venugopal, N.; Scrosati, B.; Sun, Y.-K. A High Energy and Power Density Hybrid Supercapacitor Based on an Advanced Carbon-Coated $Li_4Ti_5O_{12}$ Electrode. *J. Power Sources* **2013**, *221*, 266–271.
55. Aravindan, V.; Chuiling, W.; Madhavi, S. High Power Lithium-Ion Hybrid Electrochemical Capacitors Using Spinel $LiCrTiO_4$ as Insertion Electrode. *J. Mater. Chem.* **2012**, *22*, 16026–16031.

56. Karthikeyan, K.; Kim, S. H.; Kim, K. J.; Lee, S. N.; Lee, Y. S. Low Cost, Eco-Friendly Layered $Li_{1.2}(Mn_{0.32}Ni_{0.32}Fe_{0.16})O_2$ Nanoparticles for Hybrid Supercapacitor Applications. *Electrochim. Acta* **2013**, *109*, 595–601.
57. Jo, C.; Hwang, J.; Song, H.; Dao, A. H.; Kim, Y.-T.; Lee, S. H.; Hong, S. W.; Yoon, S.; Lee, J. Block-Copolymer-Assisted One-Pot Synthesis of Ordered Mesoporous WO_{3-x}/Carbon Nanocomposites as High-Rate-Performance Electrodes for Pseudocapacitors. *Adv. Funct. Mater.* **2013**, *23*, 3747–3754.